Nanoscale Advances

ROYAL SOCIETY OF CHEMISTRY

PAPER

View Article Online
View Journal | View Issue

Cite this: *Nanoscale Adv.*, 2025, **7**, 1923

A multistimuli responsive and self-healing Zn(II)–inosine supramolecular metal–organic gel: phase selective gelation and application as a light-responsive Schottky barrier diode†

Surbhi Singh,[a] Atul Kumar Sharma,[b] Kunal Rohilla,[a] Nisha Verma[a] and Bhagwati Sharma *[a]

Utilization of naturally available biomolecules such as nucleosides with several coordination sites as organic counterparts for the synthesis of multifunctional self-assembled metal–organic gels is important, considering the time and efforts required for the design of organic ligands that can coordinate to metal ions, forming a gel. In the present work, inosine, a simple nucleoside has been utilized as a ligand for the generation of a supramolecular metallo-hydrogel through coordination with Zn^{2+} ions in the presence of NaOH. Several spectroscopic, microscopic and rheological investigations have been performed to characterize the formed gel. The obtained metallo-hydrogel is transparent, and the transparency can be tuned depending on the amount of NaOH used. The Zn–inosine metal–organic gel exhibits several functional properties such as self-healing, stimuli responsiveness, thixotropy, and injectability. Furthermore, the freeze-dried Zn–inosine xerogel exhibited selective gelation of water, which has been utilized to separate water from mixtures that include organic solvents (or oils) and water. The semiconducting characteristics of the Zn–inosine metallogel have been used for device fabrication based on the Schottky diode interface between a semiconductor and metal. The fabricated device was found to be photo-responsive in nature and exhibited better device parameters when illuminated with light. The present results are anticipated to lead to the development of newer soft materials constructed using simple biomolecules for environmental and electronic applications.

Received 29th December 2024
Accepted 17th January 2025

DOI: 10.1039/d4na01079e

rsc.li/nanoscale-advances

1. Introduction

Supramolecular gels constitute an important category of soft materials due to their multifunctional applications in numerous fields such as catalysis, sensing, optoelectronics, drug delivery, tissue engineering, the environment and energy.[1–12] Such gels can entrap a large volume of solvent and thus can mimic soft tissues. Supramolecular gels are constructed using compounds with low molecular weight that can self-assemble into nanostructures with the help of various noncovalent interactions such as H-bonding, coordination, pi–pi stacking, electrostatic and hydrophobic interactions.[13–17] Supramolecular gel formation is usually triggered by the use of external forces like heating–cooling or sonication. The gel formation can also be triggered by incorporating metallic components such as metal ions or metal–organic components with the building blocks. The metallic components can also establish additional interactions within the building blocks and result in the self-assembly of organic building blocks, leading to the formation of metallogels.[18,19] Furthermore, the formation of metallogels is an attempt to blend the physico-chemical properties of metallic components with the soft unique features of the organic linker to generate a hybrid material with superior properties.[20,21] The dynamic metal–ligand coordination interaction in metallogels can easily be deformed and reformed, as a result of which several metallogels have demonstrated self-healing and stimuli-responsive properties.[22–25] However, designing organic linkers that can coordinate with metal ions to generate metallogels is often time-consuming, costly, and cumbersome.[26,27] Therefore, researchers have focused on the use of readily available and cost-effective small biological molecules as ligands for the formation of metallogels. Small biological molecules such as amino acids, nucleobases, nucleosides, nucleotides, *etc.* are promising materials for metallogel formation due to the presence of multiple H-bonding as well as coordination sites to which the metal ions can coordinate.[28–30] Nevertheless, limited literature is available that has shown the utilization of naturally occurring, unmodified biomolecules as

[a]*Materials Research Centre, Malaviya National Institute of Technology Jaipur, Malviya Nagar, Jaipur 302017, India. E-mail: bhagwati.mrc@mnit.ac.in*

[b]*Department of Electronics and Communication Engineering, Malaviya National Institute of Technology Jaipur, Malviya Nagar, Jaipur 302017, India*

† Electronic supplementary information (ESI) available. See DOI: https://doi.org/10.1039/d4na01079e

organic ligands for the formation of metallogels, and the use of biomolecules for metallogel formation is still in its infancy.[31–38] Furthermore, the generation of a metal-biomolecule supramolecular gel that selectively gelates an organic or aqueous solvent is advantageous for applications such as the recovery of oil spills or the removal of water from organic solvents/oils.[39–42] Therefore, the development of phase-selective supramolecular gels that can be converted to xerogels and have the ability to swell upon the addition of solvent is an area of utmost interest.

Metallogels have found widespread use in various applications related to health, energy, and the environment. The presence of metal ions in metallogels can improve the conductivity of the system, endow them with excellent charge transport properties, and make them potential candidates for the fabrication of electrical and optoelectronic devices.[4,43–46] One of the important parts of such devices, which is critical for the performance and proper functioning of the device, is the metal–semiconductor (MS) junction. Schottky barrier diodes (SBDs), an important optoelectronic device with a low operational voltage, and lower barrier height are considered to be superior to the conventional p–n junction. In a typical SBD, a metal functions as the Schottky layer, while a semiconductor functions as the drift layer. Although, supramolecular gels promise to be an ideal candidate for the formation of SBDs,[45,47–51] their utilization for soft electronic applications has been limited largely due to the non-conductive nature of the formed gel.

Herein, we report our results on the fortuitous formation of a supramolecular metallo-hydrogel based on the interaction of a commonly available nucleoside, inosine, with Zn^{2+} ions. Inosine was chosen as a ligand, as it has three possible metal coordination sites and a few H-bonding sites. Zn^{2+} ions were the metal ions of choice, because they are relatively inexpensive, have semiconducting characteristics, and are utilized in energy and power storage devices. Although the nucleotide inosine-5′-monophosphate (IMP) is known to form a metallogel upon interaction with Ag^{+} ions,[42] pure unsubstituted inosine has not been used as a ligand for metallogel formation. The gel formation is instantaneous and occurs at room temperature in a few minutes. The Zn–inosine (Zn–I) hydrogel was transparent and exhibited stimuli responsiveness towards pH and chemicals. Moreover, the Zn–I gel was self-healing in nature and also exhibited thixotropic and injectable properties. The gel was semiconducting in nature and has been utilized for the fabrication of a photosensitive SBD with excellent device parameters in the presence of light. The freeze-dried Zn–I xerogel had the unique capability to swell up upon the addition of water, which has been utilized for the phase-selective gelation of water in a water–organic solvent mixture.

2. Experimental section

2.1 Materials

All the transition metal salts (manganese chloride, cobalt chloride, ferric nitrate nonahydrate, nickel chloride, zinc acetate dihydrate, zinc nitrate hexahydrate and zinc chloride), phytic acid, inosine, guanosine, adenosine, thymidine, cytidine, uridine, methylene blue and rhodamine B were procured from Sisco Research Laboratories, India. The lanthanide metal salts (erbium chloride, neodymium chloride, samarium chloride, terbium chloride, dysprosium chloride, praseodymium chloride, and gadolinium nitrate), and lithium hydroxide were procured from Sigma-Aldrich. Ethylenediaminetetraacetic acid (EDTA), trifluoroacetic acid (TFA), imidazole, ammonia, sodium hydroxide, ethanol, hexane, hydrochloric acid, and nitric acid were bought from Merck, India. Potassium hydroxide was procured from Fisher Scientific. All the chemicals were used as received, without any additional purification. MilliQ water was utilized in all the experiments.

2.2 Instrumentation

Field Emission Scanning Electron Microscopy (FESEM) images were obtained on a Nova Nano FESEM 450 that was purchased from FEI. The sample was loaded after coating it with gold in order to make it conductive. Transmission electron microscopy (TEM) images have been acquired using a Tecnai G2 20 S-TWIN electron microscope from FEI. The rheological investigations on the gel were carried out with a rheometer from Anton Paar (MCR 302) utilizing a parallel plate geometry (50 mm). A PerkinElmer LAMBDA-750 UV-visible-NIR spectrophotometer was used to perform the UV-visible studies. The FTIR studies were performed on a PerkinElmer FTIR spectrometer (Spectrum-2) in KBr pellet mode. X-ray photoelectron spectroscopy studies were performed on Omicron Nanotechnology equipment with Al Kα (1486.7 eV) as the X-ray source. Mass spectrometric analysis was conducted using a high-resolution mass spectrometer (Xevo G2-S QTof) from Waters, USA. A sourcemeter (Keithley 2450) was utilized to investigate current–voltage (*I–V*) characteristics of the fabricated SBD. An SDA probe station (B1500A) supplied by Agilent Technologies was used to assess the device parameters.

2.3 Synthesis of the Zn–inosine metallo-hydrogel

The Zn–inosine hydrogel was synthesized by mixing aqueous solution of the metal salt and aqueous alkaline solution of inosine. Briefly, inosine solution (0.1 M) was prepared by dissolution of 26.8 milligrams of inosine in 1.0 mL of alkaline water (0.82 mL H_2O + 0.18 mL NaOH (1 M)). Another solution (0.1 M) containing the zinc salt (acetate/nitrate/chloride) was prepared by simply solubilizing the respective metal salt in water. To obtain the Zn–inosine hydrogel, both the above solutions were mixed in a 1 : 1 ratio (v/v) in a glass vial and kept for three hours without being disturbed.

2.4 Electron microscopic studies

The sample for FESEM was prepared by dilution of the gel sample using water. A piece of gel was taken in a 2 mL tube with the help of a microspatula. 0.5 mL of water was then added to the tube. A micropestle was then used for crushing the gel in water, followed by shaking the tube. The resulting dispersion (50 μL) was then dropcast on a cleaned glass slide (1 cm × 1 cm) and left for drying for 24 h at room temperature in a desiccator. The sample for TEM was prepared by placing a small fraction of the gel onto a carbon coated Cu grid. The gel piece was removed

from the grid after 5 minutes and the grid was dried for 24 h at room temperature.

2.5 Rheological analysis

The rheological studies of the as-synthesized gel were performed using 1.0 mL of Zn–inosine gel utilizing a parallel plate geometry (50 mm). The hydrogel was taken out from the tube and placed on the plate of the rheometer using a clean spatula. The experiment was carried out maintaining a temperature of 25 °C. To perform the dynamic strain sweep studies, a constant frequency of 10 rad s^{-1} was used. The frequency sweep measurements were performed at a constant strain of 1% with the angular frequency being varied from 0.05–100 rad s^{-1}. Thixotropic measurement was performed by successive application of maximum (100%) and minimum (0.1%) strains at a definite time duration at 25 °C.

2.6 Electro-spray ionization mass spectrometric (ESI-MS) analysis

ESI-MS investigation of the Zn–inosine gel was carried out in water. Briefly, 20 mM aqueous solution of inosine (in NaOH) was prepared by diluting the stock solution (100 mM) prepared by dissolution of 26.8 mg inosine in alkaline water. Separately, an aqueous solution of $Zn(CH_3COO)_2$ with a strength of 20 mM was prepared. Both the solutions were mixed in a 1 : 1 ratio (v/v), resulting in a clear solution. This transparent solution was then incubated for 60 minutes at room temperature and ESI-MS studies were performed. HPLC grade water was used for the preparation of samples for ESI-MS studies.

2.7 Determination of Zn : inosine stoichiometry using Job's plot

The stoichiometry (metal : ligand) in the Zn–inosine complex was evaluated using Job's plot. 5×10^{-5} M aqueous solutions of both inosine (in NaOH) and $Zn(CH_3COO)_2$ were used for constructing the plot. The UV-visible spectrum of the solutions prepared by varying the mole fraction of both the ligand and $Zn(CH_3COO)_2$ was recorded. The stoichiometry was determined by plotting $\Delta A \times \chi_L$ against χ_L, where ΔA represents the change in absorbance and χ_L is the mole fraction of inosine.

2.8 Self-healing studies

To study the self-healing nature of the as-synthesized gel, the Zn–I gel was carefully taken out from the glass vial and placed on a Petri dish. The gel was cut into two equal pieces. Then both the gel pieces were brought close to each other and slightly pressed and left undisturbed for 1 h to allow for the self-healing process. Rh B dye doping was used for clarity in one of the blocks of gel.

2.9 Stimuli responsiveness of the Zn–I gel

The stimuli responsiveness of the Zn–I gel was investigated by subjecting the hydrogel to variety of chemicals and pH, and observing the transition from a gel to the sol state visually. Briefly, 1.0 mL of the gel was prepared in a glass vial, and acids/bases and chemicals with different concentrations were added to the gel, and the visual outcome was noted.

2.10 Phase selective gelation and separation of water from oils/organic solvents

The Zn–I xerogel possessed the unique property to selectively gelate water and swell, which was used for separating water selectively from a mixture of water and organic solvents. The Zn–I xerogel was obtained by lyophilization of the Zn–I hydrogel. The freeze-dried xerogel (50 mg) was mixed with a mixture containing 1 mL of water and 1 mL of hexane. For better visualization, Rh B dye was mixed with the water fraction. The mixture was kept undisturbed for 8 h, when the water fraction containing the dye was gelled, leaving behind the hexane fraction. A conventional decantation could be used to retrieve the hexane layer. Similar studies were performed using common oils such as pump oil, petrol, olive oil, mustard oil, silicone oil, and coconut oil, which demonstrated the applicability of the Zn–I xerogel for selective removal of water from a mixture of these oils and water.

2.11 Device fabrication

Indium-doped tin oxide (ITO) coated glass substrates were used to fabricate the electrical device. Acetone and deionized water were used to wash the ITO substrate after it had been ultrasonically cleaned using a soap solution. Spin coating was used for two minutes at 1000 rpm and then for two minutes at 1500 rpm to coat the supramolecular Zn–inosine metallogel on the ITO-coated glass substrate. In a vacuum oven, the thin films were subjected to drying for a short while at 100 °C. The thicknesses of the thin films that were formed were determined to be around 1 μm by use of a surface profilometer. With thermal coating equipment, the silver metal electrode for the contact electrode was deposited. The spherical dots on the surface of the metal electrodes (Ag) were deposited using a shadow mask.

3. Results and discussion

3.1 Synthesis of the Zn–inosine metallo-hydrogel

The formation of the Zn–I gel could be achieved by simple mixing of an aqueous $Zn(CH_3COO)_2$ solution (100 mM) and an alkaline inosine solution (100 mM, pH 12.4). Initially, a turbid sol was formed upon mixing both components, which transformed into a transparent gel within 30 minutes of standing (Scheme 1). This suggested that the coordination between Zn^{2+} ions and inosine followed a fast kinetics, and the Zn^{2+} ions triggered the self-assembly of inosine into ordered nanostructures that could trap water molecules. It was interesting to note that unlike many of the reported supramolecular gels, the Zn–I gel formation did not require the assistance of external conditions such as sonication or heating–cooling,[52,53] and the gel formation occurred at room temperature. The hydrogel formation was initially confirmed by the tube inversion method, which prevented the flow of the mass under gravity (inset of Fig. 1a). It is important to mention that only Zn^{2+} ions could

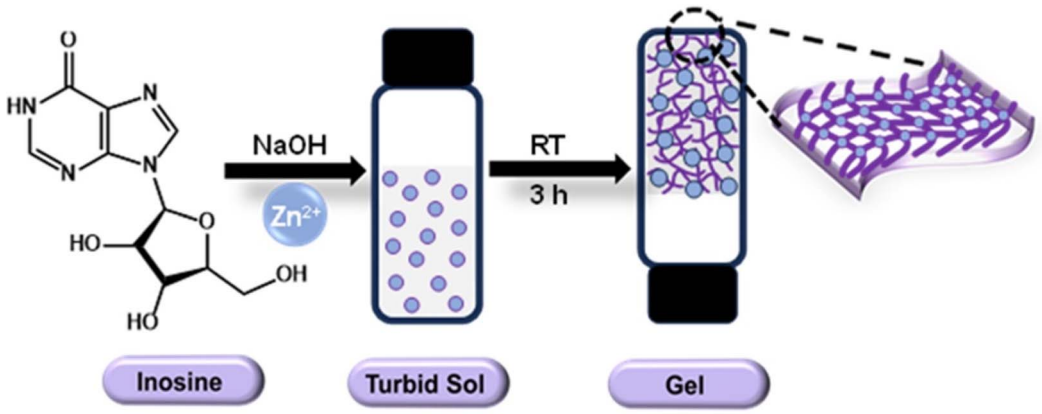

Scheme 1 Schematic representation of Zn–inosine hydrogel formation using Zn^{2+} ions and alkaline solution of inosine at room temperature.

form a gel with inosine. Using other common transition or lanthanide metal ions resulted in the formation of either precipitates or clear solution (Fig. S1†). The specificity of Zn^{2+} ions towards gel formation could be attributed to higher-ordered self-assembly in the Zn^{2+}–inosine system through multivalent crosslinking induced by Zn^{2+} ions, which is not possible with other metal ions.[54] The Zn–I gel was stable for months as no observable change was noticed even after standing for months (Fig. S2†). The Zn–I gel, unlike many supramolecular gels, exhibited stability even at temperatures greater than 90 °C without showing any visual change or solvent leakage.

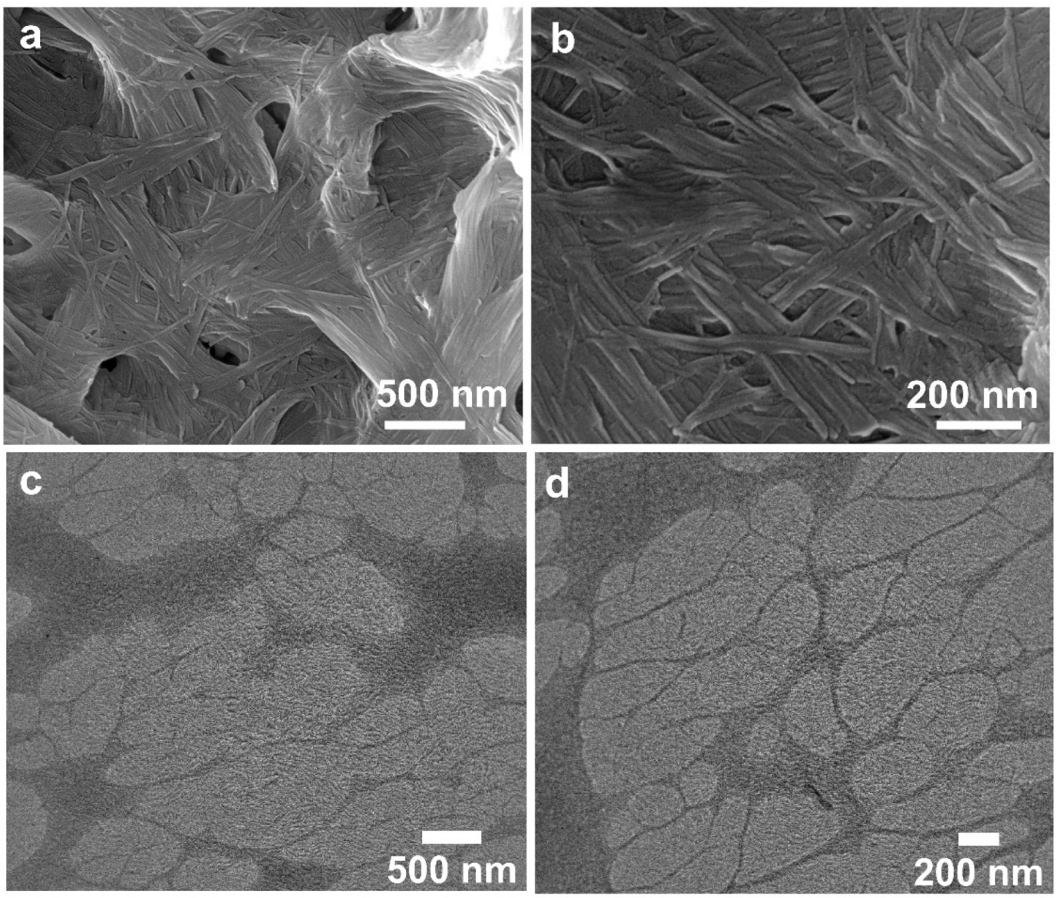

Fig. 1 (a) FESEM image showing the entangled fibrous network-like morphology of the Zn–inosine gel (inset: digital image of a transparent Zn–inosine gel, showing the absence of flow upon tube inversion), (b) magnified FESEM image, (c) TEM image, and (d) higher magnification TEM image showing the nanofibrous morphology of the Zn–inosine gel.

3.2 Morphological characterization of the Zn–inosine hydrogel

We employed electron microscopic techniques to understand the morphology of nanostructures responsible for Zn–I metallo-hydrogel formation. The FESEM images of the Zn–I hydrogel demonstrated the formation of intertwined nanofibers (Fig. 1a and b). The diameter of individual fibers was calculated to be 40–60 nm and the length was calculated to be in the micrometer regime. The TEM images of the hydrogel further validated the formation of nanofibers. These nanofibers through entanglement led to the formation of a three-dimensional network of fibers (Fig. 1c and d). The diameter of the nanofibers calculated using the SEM images was comparable to those obtained using the TEM images. The water molecules can understandably be immobilized by the nanofibers forming such a dense network.

3.3 Rheological studies

The viscoelastic nature and the mechanical stability of the Zn–I gel were evaluated using rheological measurements. From the strain sweep rheological measurement, it was found that the value of the elastic storage modulus (G') was considerably higher than the loss modulus (G'') up to a strain of 19%, indicating the dominance of elastic solid-like behaviour of the Zn–I gel over liquid like viscous nature (Fig. 2a). However, beyond a strain of 19%, the viscous nature dominated the elastic behavior, as evidenced by the larger values of G'' than G',[32] indicating the conversion from the gel to the sol state at strain values greater than 19%. Furthermore, the frequency sweep rheological investigation also ascertained the supremacy of the elastic solid-like nature over the viscous behavior of the Zn–I hydrogel (Fig. 2b). The values of G' were higher than G'' by an order of magnitude in the whole frequency range (0.1–100 rad s^{-1}). Next, we studied the thixotropic behavior of the Zn–I metallo-hydrogel to investigate the role of strain in the mechanical properties of the Zn–I gel during a defined time period, by escalating the strain value to a maximum and then decreasing back to the initial lower strain at 25 °C during the time limit (Fig. 2c). We sequentially applied the maximum (100%) and minimum (0.1%) strain at specific gaps. The strain value was varied so that at higher strain values (100%) the gel could completely lose the elastic behavior ($G'' > G'$) and upon decreasing the strain (0.1%), the elastic nature could be regained ($G' > G''$). As expected, upon application of 0.1% strain, the values of G' dominated those of G'' by 1 order of magnitude. However, when we increased the strain to 100%, it was observed that the viscous behavior of the Zn–I gel dominated the solid like elastic nature. Upon decreasing the strain back to the minimal value (0.1%), it was found that the elastic nature again dominated the viscous behavior. Such cycles could be repeated

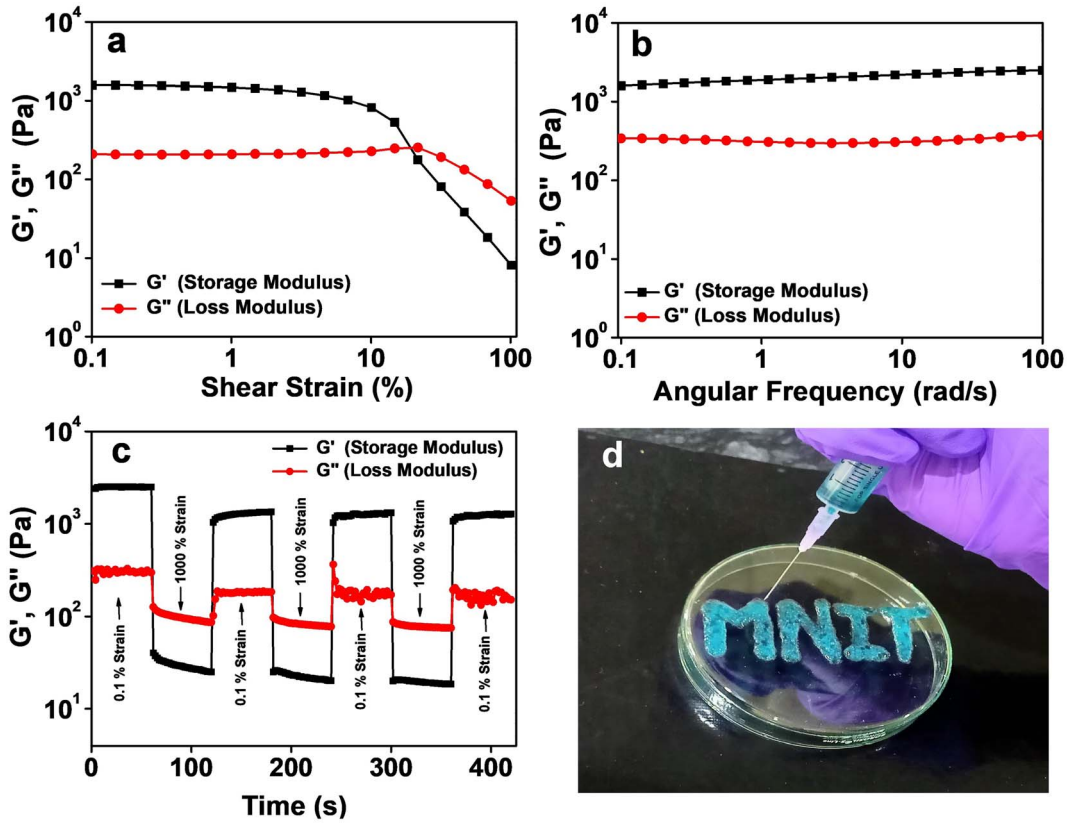

Fig. 2 Rheological studies of the Zn–inosine metallo-hydrogel, (a) strain sweep rheology of the Zn–I gel up to a strain of 100%, and (b) frequency sweep rheology of the Zn–I gel performed by fixing the strain at 1%. (c) Thixotropic loop test of the Zn–I hydrogel performed *via* continuous step-strain measurement with a fixed angular frequency (10 rad s^{-1}) and (d) digital image showing the injectable properties of the Zn–I gel. The gel has been doped using methylene blue dye for clarity.

several times. It was found that up to 75% of the G' value could be recovered after three cycles, which indicates that the material has the potential to be used as an injectable soft material. The thixotropic nature of the Zn–I gel inspired us to evaluate its injectable properties. As can be seen from Fig. 2d, the Zn–I hydrogel could be pulled using a syringe easily and is injectable in nature, suggesting its potential in drug delivery applications.

3.4 Spectroscopic characterization

The stoichiometry of Zn^{2+} : I in the formed gel was evaluated using UV-visible studies. The mole fractions of the Zn^{2+} ions and inosine were varied to construct a Job's plot, which suggested a stoichiometry of 1 : 1 between Zn^{2+} ions and inosine (Fig. S3†), in accordance with the formation of the stable get at a 1 : 1 molar ratio of both components. FTIR measurements were carried out to understand the coordination of Zn^{2+} ions to inosine (Fig. S4†). The FTIR spectrum of pure inosine displayed a weak band at 3537 cm^{-1} and a medium intensity band at 3384 cm^{-1} attributed to O–H stretching vibration in the sugar moiety. In the case of Zn–I, both these bands were not observed, and a broad band with strong intensity at 3435 cm^{-1} was noticed, which indicated the presence of water molecules in the Zn–I xerogel. Furthermore, the strong intensity band at 1696 cm^{-1} due to C=O stretching vibrations in inosine shifted to 1632 cm^{-1} with a decrease in intensity in the Zn–I gel, indicating the probable role of the C=O group in either H-bonding or binding to Zn^{2+} ions. Furthermore, the peak at 1592 cm^{-1} due to C=N stretching of the purine ring almost completely disappeared suggesting the involvement of the purine ring in metallation. The changes in the stretching vibrations of the C–N bond of the imidazole ring from 1352–1425 cm^{-1} further confirmed the binding of the metal ion to the purine ring of inosine.[42] The oxidation state of zinc in the Zn–I gel was probed using X-ray photoelectron spectroscopy (XPS). The XPS survey spectrum of the Zn–I xerogel showed the presence of C 1s, N 1s, O 1s, and Zn 2p at their characteristic binding energies (Fig. S5a†). The high-resolution XPS spectrum of Zn 2p showed the presence of peaks at 1045.6 and 1022.4 eV, characteristic of Zn $2p_{1/2}$ and Zn $2p_{3/2}$ (Fig. S5d†), respectively. The difference of 23.2 eV between the two binding energies confirmed the presence of zinc in the +2 oxidation state.[55] ESI-MS of the viscous aqueous mixture obtained by mixing inosine in NaOH (20 mM) and $Zn(CH_3COO)_2$ (20 mM) in a 1 : 1 ratio (v/v) showed an intense peak at a m/z value of at 468.7228 (Fig. S6†), indicating the formation of $ZnI(CH_3COO)(H_2O)_3$. This basic unit of the complex can coordinate to another inosine unit through Zn^{2+} ions, and result in chain extension, forming nanofibers.

3.5 Control experiments

Next, we performed several control experiments to establish the conditions suitable for stable Zn–I gel formation. It was found that the lowest concentration of both reactants that could result in gel formation was 40 mM (Fig. S7†). Below a concentration of 40 mM, only a viscous sol was formed. The SEM image of viscous sol obtained using a 20 mM concentration of both the reactants also showed the formation of nanofibers (Fig. S8†). Nevertheless, a higher concentration of the reactants (>40 mM) was necessary for gel formation. It was found that using a molar ratio of both components of 1 : 1 (0.1 M : 0.1 M) resulted in the formation of the most stable gel (Table S1†). When the concentration of Zn^{2+} ions was changed, keeping the concentration of inosine constant (0.1 M), a rather weak gel was formed (as observed physically). Similar results were obtained when the concentration of Zn^{2+} ions was kept constant (0.1 M), and the molar ratio of inosine was varied. Furthermore, it was also confirmed that gel formation only occurred under alkaline conditions, as at a neutral or acidic pH, only a transparent solution was observed (Fig. S9†). We also studied the interactions of other commonly available nucleosides, adenosine, cytidine, thymidine, uridine, and guanosine, with Zn^{2+} ions under similar conditions. It was found that gel formation occurred only with inosine and guanosine, which was expected as the ability of inosine and guanosine to form complexes is the highest among all the nucleosides.[56] A turbid sol was observed in the case of all other nucleotides under similar conditions (Fig. S10†). Next, metal counterions were varied to investigate their role in stable gel formation. A stable gel was observed in all the cases (Fig. S11†), confirming that the change in metal counterions did not affect the gelation. The SEM images indicated the formation of a network of fibers and an intertwined web-like structure when $Zn(NO_3)_2$ and $ZnCl_2$ were used as metal salts, respectively (Fig. S12†). We also studied the interaction of inosine and Zn^{2+} ions under similar conditions in methanol and ethanol. However, instead of a gel, a precipitate was observed when pure methanol or ethanol was used as a solvent (Fig. S13†). Next, the gelation studies were carried out in mixed solvent systems, wherein inosine was dissolved in water, while the metal ion was solubilized in methanol or ethanol. An opaque gel was observed in both cases (Fig. S13†), implying the possible role of water molecules in H-bonding that assists the gel formation. We also changed the base from NaOH to LiOH and KOH to understand if the gel formation was specific to a particular base. However, in all three cases, a transparent gel was formed (Fig. S14†), implying that the gel formation was not specific to any particular base.

3.6 Possible mechanism for gel formation

Based on all the above results, we propose the following plausible mechanism for the formation of the Zn–I hydrogel. At alkaline pH, deprotonation of the hydrogen at the N1 position of inosine results in the conversion of the keto form of inosine to the enol form. The Zn^{2+} ions can coordinate to the oxygen atom *via* the lone pair electrons on the oxygen atom. Another Zn^{2+} ion then coordinates with the N7 of the inosine unit and is, in turn, again bound with the oxygen atom of another inosine unit, thus extending the chain to form a polymeric network. Furthermore, other non-covalent interactions, such as π–π stacking between individual strands and H-bonding, assisted the formation of an entangled network of nanofibers that have the capability of trapping the water molecules, resulting in the formation of a hydrogel (Scheme 2). It is, however, imperative to mention that Zn^{2+} ions tend to form $Zn(OH)_2$ clusters at a basic

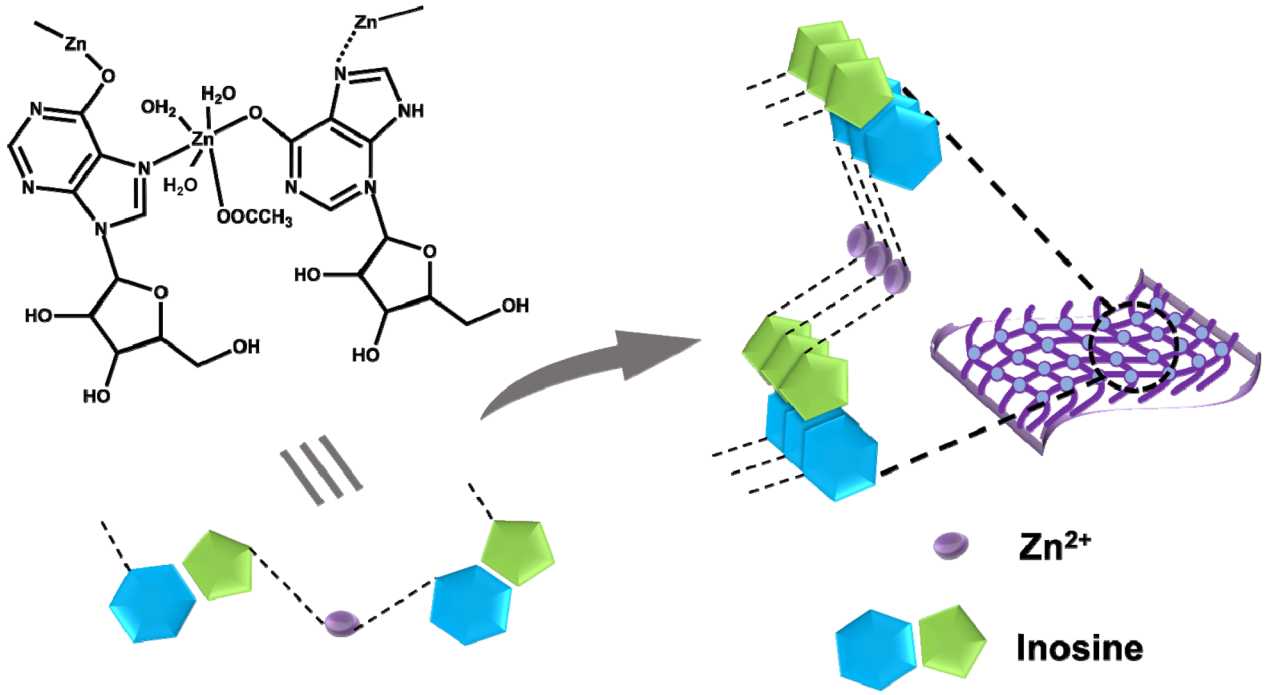

Scheme 2 Proposed structure of the complex resulting from the interaction of Zn^{2+} ions and inosine, and schematic representation of the assembly of the complex into fibers assisted by other non-covalent interactions.

pH. Therefore, the possible role of $Zn(OH)_2$ clusters in binding to inosine, leading to the formation of the stable gel cannot be ruled out. To understand the role of pH and $Zn(OH)_2$ clusters in stable gel formation, we performed the gelation of the Zn–inosine system at varying pH values ranging from 7 to 14 (Fig. S15†). It was found that at a pH of 7–9, there is no observable interaction between inosine and Zn^{2+} ions, as a clear sol is obtained upon interaction of Zn^{2+} ions with inosine at this pH. However, as the pH is increased to 10 (or 11), the interaction between the metal and inosine is visible, as revealed by the increased viscosity of the clear sol. Furthermore, as the pH is increased to 12.5, the interactions between inosine and Zn^{2+} ions are more favorable, as indicated by the formation of a self-standing transparent metallo-hydrogel. Upon further increasing the pH, an opaque gel was obtained, suggesting the possible formation of $Zn(OH)_2$ clusters in the Zn–I gel, resulting in opaque gel formation. To confirm if $Zn(OH)_2$ clusters are actually formed in any of the gels (gel with inosine at pH 12.5 (L1) and gel with inosine at pH 13.3 (L2) (Table S2†)), we performed the powder X-ray diffraction (PXRD) studies on both the freeze-dried xerogels. The PXRD pattern (Fig. S16†) showed an amorphous nature of the L1 gel and the peaks corresponding to $Zn(OH)_2$ could not be observed in the sample. This indicated that $Zn(OH)_2$ does not form in the case of L1, which is also evident from the transparency of the L1 gel. However, in the case of a freeze dried L2 gel, we did observe some crystalline peaks, although those could not be indexed to $Zn(OH)_2$, suggesting that $Zn(OH)_2$ is not formed in any of the gels. Furthermore, although the pH of the inosine solution before addition of $Zn(CH_3COO)_2$ is ~12.5 for the formation of a transparent Zn–I gel, the pH after the addition of equimolar $Zn(CH_3COO)_2$ (resulting in gel formation) decreases to ~7.0, which further rules out the possibility of the formation of $Zn(OH)_2$. Therefore, the only interaction responsible for gelation in the present case is the coordination interaction between Zn^{2+} ions and inosine.

Furthermore, to verify that $Zn(OH)_2$ alone is incapable of gelling water, we performed the reaction using varying amounts of NaOH in the absence of inosine. In all the cases, only a white precipitate rather than a gel was observed (Fig. S17†), clearly indicating that only $Zn(OH)_2$ cannot gel the water. Thus the gel formation in the present case is due to the coordination of inosine with Zn^{2+} ions.

3.7 Stimuli responsiveness of the Zn–I gel

The weak non-covalent interactions that play a critical role in metallogel formation can often be modulated by application of appropriate stimuli such as chemicals, pH or heat.[24,53] Under the influence of these stimuli, the coordination bond between the metal ion and the ligand can be deformed leading to a gel to sol transition. However, upon removal of such stimuli, the sol to gel transition can be restored. In the present case also, it was observed that the Zn–I gel exhibited multiple stimuli responsiveness towards pH and chemicals (Fig. 3). We observed that adding a few drops of 1 M hydrochloric/nitric acid to the transparent Zn–I gel resulted in the collapse of the gel in a few minutes. Nevertheless, the gel-to-sol transition could be reversed when an equivalent amount of base (NaOH) was added. The findings indicate that in the presence of an acid, the dynamic coordination interaction between Zn^{2+} ions and inosine is broken which results in the gel-to-sol transition.

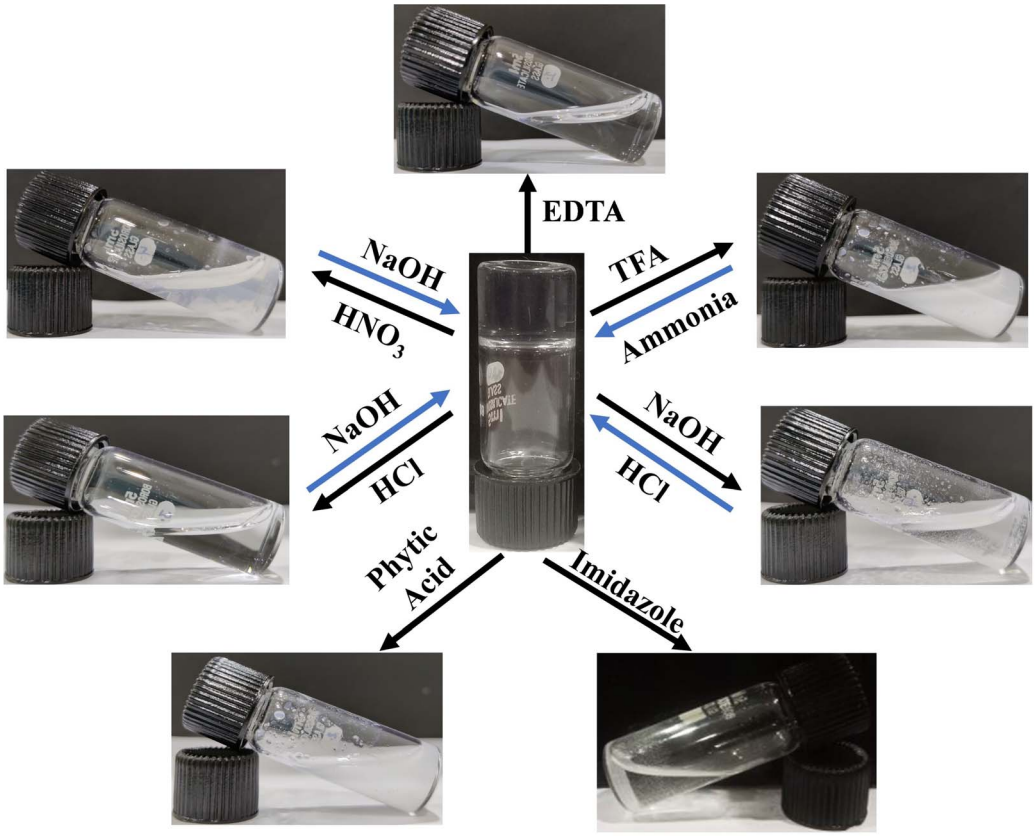

Fig. 3 Digital images demonstrating the stimuli responsiveness of the Zn–inosine metallo-hydrogel towards pH and chemicals.

Furthermore, when an equivalent amount of the base is added to the sol, the interactions can reform resulting back in the gel state. We observed a similar gel-to-sol transformation, when 100 μL of a mild acid (4 M TFA) was added to 1.0 mL of the gel. The sol to gel transition can be recovered by adding an appropriate amount of NH_4OH. Next, we studied the effect of the addition of 1 M NaOH to the gel, which resulted in the transformation of the gel into a turbid sol. The gel could, however, be recovered by adding an equivalent amount of acids (HCl/HNO_3). The Zn–I gel also exhibited responsiveness towards chemicals such as EDTA, phytic acid, and imidazole. The addition of EDTA (or phytic acid or imidazole) resulted in the transition of the Zn–I gel to the sol state, which could be ascribed to the higher affinity of EDTA to Zn^{2+} ions as compared to inosine. Due to the higher affinity, EDTA can displace the inosine from the Zn–I complex, resulting in the formation of the sol. All the findings suggested that the coordination bond in the Zn–inosine complex is dynamic and can be changed depending on the environment and chemicals.

3.8 Self-healing and transparency of the Zn–inosine gel

The presence of dynamic non-covalent interactions in the Zn–I gel and the excellent thixotropic nature of the Zn–I metallo-hydrogel, as indicated by the rheological studies prompted us to evaluate the self-healing nature of the Zn–I gel. The self-healing behavior of the Zn–I gel was studied by cutting and splitting the gel block into two halves (Fig. 4a). The cut gel blocks were brought close to each other and pressed slightly, and left undisturbed. Interestingly, the blocks of the hydrogel healed at the place of cut within three hours to give a single block, without the aid of any other external healing agents, clearly signifying the inherent self-healing capability of the Zn–I gel (Fig. 4b). After the healing process, it was possible to hold the block from one end and hover it in air. To ensure clarity, we added rhodamine B dye to one of the blocks, such that it was red in color. Next, we brought an alternate dye-doped and undoped block to construct one block, which could be held horizontally or vertically (Fig. 4c). Furthermore, it was noted that the molecules of rhodamine B could diffuse from the doped block to the undoped block, suggesting that there is a continuous exchange of molecules in the interface region between the two blocks. As a result of this exchange, a dynamic equilibrium is established between the constant creation of new fibers and the disruption of existing fibers, which facilitates the expansion of the network of fibers across the interface and promotes self-healing.[42] Dynamic oscillatory rheology was utilized to quantitatively study the self-healing behavior of the Zn–I gel (Fig. 4d). The gel was strained until failure and then the recovery of the gel over a period of time at a fixed strain of 0.1% was monitored, which ascertained the self-healing nature of the Zn–I gel. The values of G' were slightly lower after the healing process, possibly due to the loss of water during the failure process. Furthermore, the mechanical properties of the pristine gel and self-healed gels were also compared, and it was found that the elastic storage

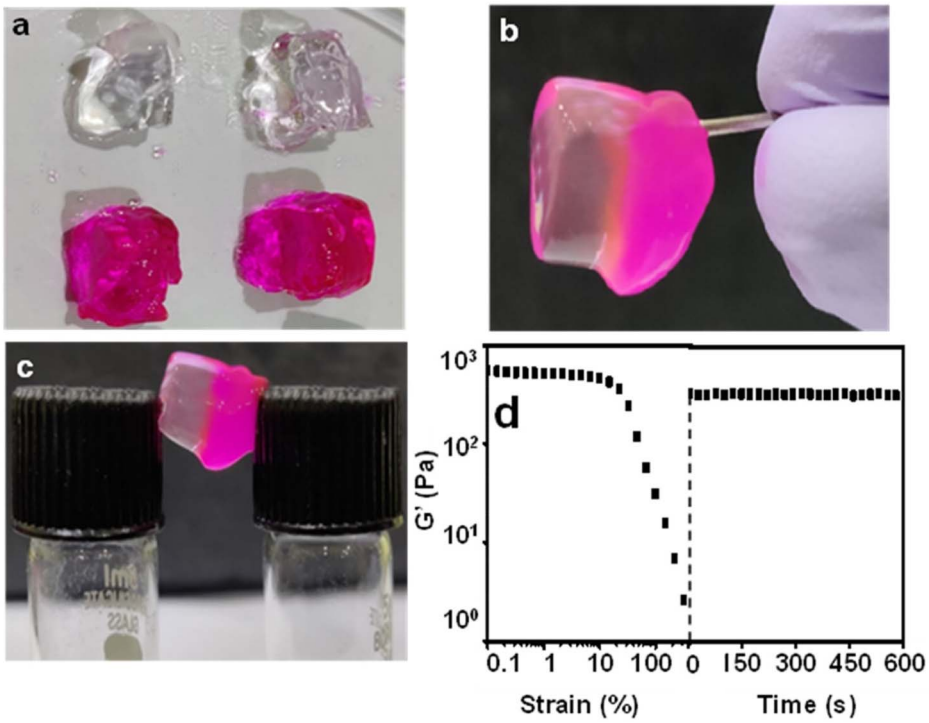

Fig. 4 Pictorial representation of the self-healing nature of the Zn–inosine metallo-hydrogel. (a) Two blocks of gel (dye-doped and undoped) cut into four pieces, (b) self-healing of two blocks into one block, and the block being held vertically, (c) self-healed metallogel single block forming a bridge, and (d) dynamic oscillatory rheological investigation confirming the self-healing ability of the Zn–inosine gel.

modulus had similar values in both cases (Fig. S18†), suggesting that the gel retained the properties during the healing process.

The Zn–I hydrogel showed excellent optical transparency, which could be tuned with the concentration of the NaOH used (Fig. S19†). When the concentration of NaOH in the inosine solution was 0.2 M, a completely transparent gel could be obtained. Below this concentration, gel formation did not occur, and only a viscous sol was obtained using a NaOH concentration of 0.15 M. On the other hand, an opaque gel was obtained when the concentration of NaOH was 0.25 M and above. The Zn–I hydrogel exhibited about 93% transmittance in the visible region (Fig. S20†). However, the transmittance in the UV region was quite weak, which signifies the potential of the Zn–I gel for applications such as UV-protective soft optical devices.[57] Furthermore, when a vial containing the gel was placed over a piece of paper, the characters were clearly legible (Fig. 5a). Similarly, when red laser light was focused on the vial containing the transparent Zn–I gel, the laser spot could be observed on the paper placed behind the vial, indicating the excellent transparency of the Zn–I gel for red light (Fig. 5b).

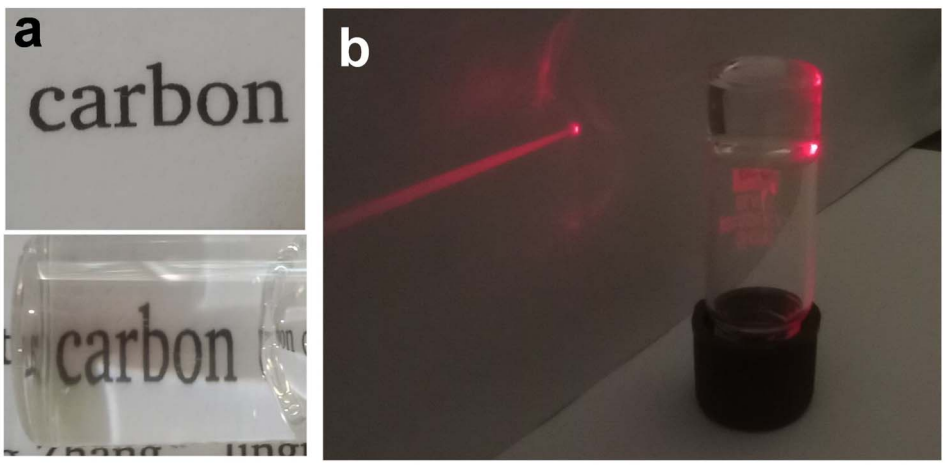

Fig. 5 (a) Digital image showing the transparent nature of the Zn–inosine gel, when placed over a piece of paper, and (b) digital image showing the transmitted red laser light through the Zn–inosine gel.

3.9 Separation of water from an oil–water mixture

The ability of a gelator to selectively gel one of the solvents in a mixture of two or more solvents, commonly known as phase selective gelation has recently attracted attention due to its technological relevance.[39,40,58–60] The use of a carbohydrate-based organogelator for the phase selective gelation of oils from an oil–water mixture has been well studied and used for environmental applications like oil spill recovery.[40,61–63] However, paucity of literature is evident with regard to the development of supramolecular small-molecule gelators that selectively gel water from a water-in-oil mixture. Such hygroscopic phase selective gelators that can gel water in an oil–water mixture are important as they can act as a desiccant to remove traces of water from liquid fuels, as the presence of water in fuels, even in trace quantities, causes serious damage to the engines. Interestingly, it was found that the addition of water to a freeze-dried Zn–I xerogel resulted in the swelling of the gel network, leading to the formation of a stable hydrogel. It was found that the swelling of the gel networks occurred only in the presence of water, and sol was obtained when non-polar solvents were added to the xerogel. It is known that the gelation ability of a gelator depends on various factors such as the solubility, H-bonding between the gelator and solvent molecules, as well as the non-specific intermolecular interactions such as the dipole–dipole interactions, *etc.*[42] Since inosine can easily be solubilized in water (in the presence of NaOH) and the presence of water allows for extended H-bonding interactions, it is highly likely that gelation of the Zn–I xerogel will be favored in the presence of water. The ability of the Zn–I xerogel to form a stable hydrogel in the presence of water was used for the separation of traces of water from common oils. It was found that the addition of the Zn–I xerogel to an oil–water mixture resulted in hydrogel formation in the water layer, while the oil layer was undisturbed. The hydrophobic layer (oil) could be separated from water by simple decantation (Fig. 6a). Furthermore, the Zn–I xerogel was also utilized to remove polar impurities such as dyes *via* the entrapment of the dye in the gel matrix. It was observed that the addition of the Zn–I xerogel to a mixture containing dye in a water and hexane mixture selectively led to the formation of the gel with the water containing the dye. Freeze drying of the hydrogel resulted in a dye-entrapped xerogel (Fig. 6b).

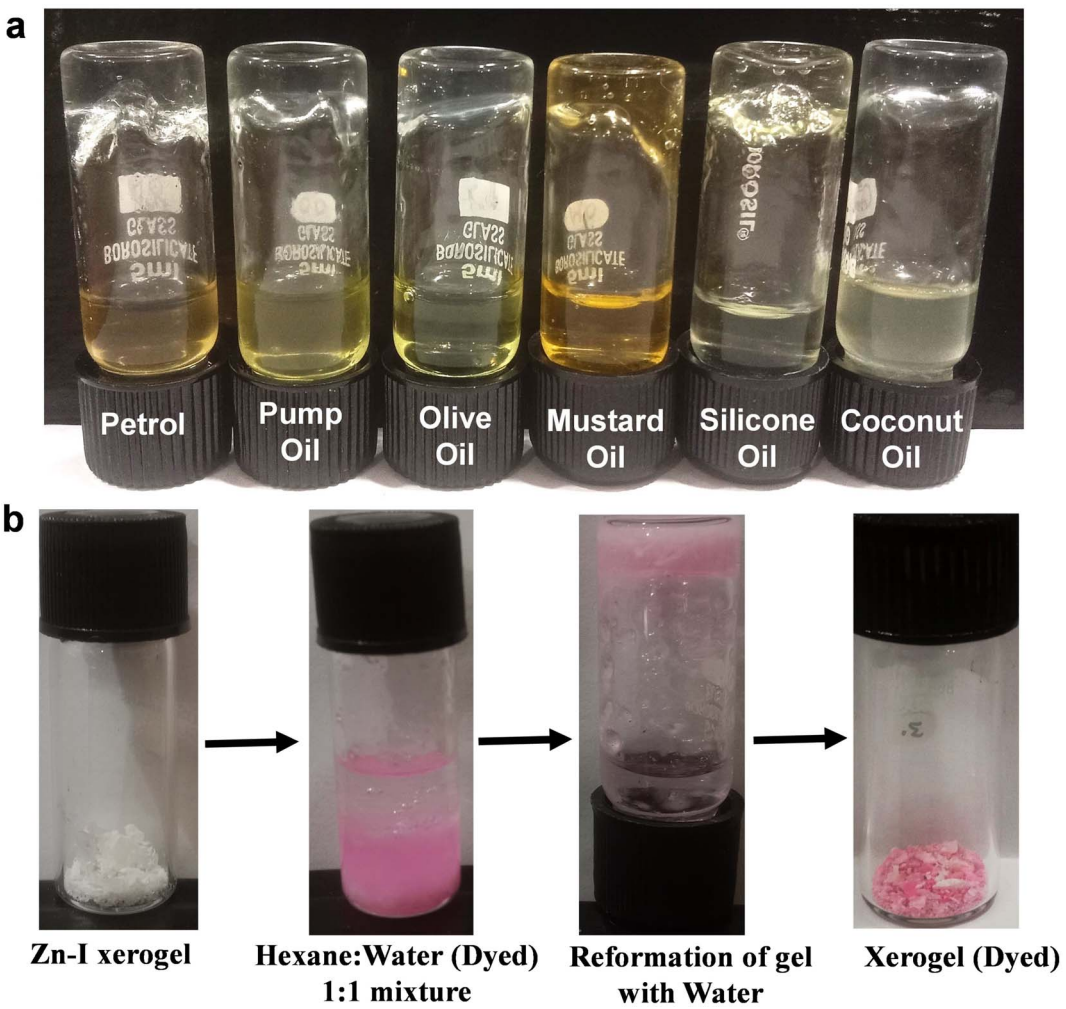

Fig. 6 (a) Digital images showing the ability of the Zn–inosine xerogel to selectively gel water in a mixture containing oil and water, and (b) photographs indicating the entrapment of dye present in a water–hexane mixture *via* gelation of the water fraction by the Zn–inosine xerogel.

3.10 Photosensitive device fabrication

Solid-state UV-visible study was carried out to analyze the nature of the Zn–I xerogel (freeze-dried). The Tauc plot was used to calculate the band gap (direct) of the xerogel, and it was found to be 3.8 eV, indicating that the Zn–I gel exhibited a semiconducting behavior (Fig. S21†). Taking advantage of the semiconducting nature of the Zn–I gel, we utilized a Zn–I gel to fabricate a thin film-coated electronic system predicated on a metal (Ag)–semiconductor (Zn–I) junction on an ITO-coated glass substrate (Scheme S1†). The *I–V* characteristics of the Zn–I gel-predicated device were studied at ambient temperature both under illumination and non-illumination of light (light intensity ~100 mW cm^{-2}) at the corresponding sequentially applied bias voltage of ±2 V. Fig. 7a displays the *I–V* characteristics of the synthesized Zn–I based device that were examined under both dark and light illuminated conditions. The electrical conductivity of the Zn–I xerogel-based electronic system was computed to be 2.15×10^{-4} S m^{-1} under non-illuminated conditions. However, in the presence of light, the electrical conductivity increased to 6.15×10^{-4} S m^{-1}, indicating the photosensitive behavior of the metallogel-based thin film device. The photoresponsivity of the device was calculated to be 2.75. The conductivity of the Zn–I gel-based device was higher than those reported for similar devices fabricated using zinc-based materials.[44,64] The increased conductivity value upon light irradiation can be attributed to the so-called "hopping transport" theory, as previously reported.[65] The *I–V* curves under both light as well as dark conditions signified non-linear rectifying behavior, typical of SBDs (Fig. 7a). The rectification ratio (I_{on}/I_{off}) at the bias voltage of ±2 V was calculated to be 34.88 and 49.25 under dark and light conditions respectively. The charge transport behavior of the Zn–I based electronic device was further probed by the analysis of the *I–V* curve by utilization of thermionic emission theory and Cheung's equation (equations in the ESI†).[66,67]

The ideality factor (η) and the series resistance (R_s) for the constructed thin film device were calculated using the intercept and slope of the plot of d*V*/dln *I vs. I* respectively (Fig. 7c). The ideality factor value under both light irradiated and non-irradiated conditions was calculated to be 2.14 and 2.48, respectively, which is far from the optimal value (~1). The departure of the value from the optimal value indicates the existence of interface states, inhomogeneities of the Schottky barrier height, and the series resistance at the junction.[68,69] Notably, under photoirradiation, the ideality factor of the metallogel-based device approaches ideality, *i.e.*, they exhibit less departure from 1. This suggests that at the interface, the recombination of charge carriers is low, and homogeneity at the Schottky junction barrier upon photoirradiation improves.

Next, we utilized the plot of *H*(*V*) *vs. I* (Fig. 7d), where *H*(*V*) is the Cheung function (detailed equations in the ESI†) to

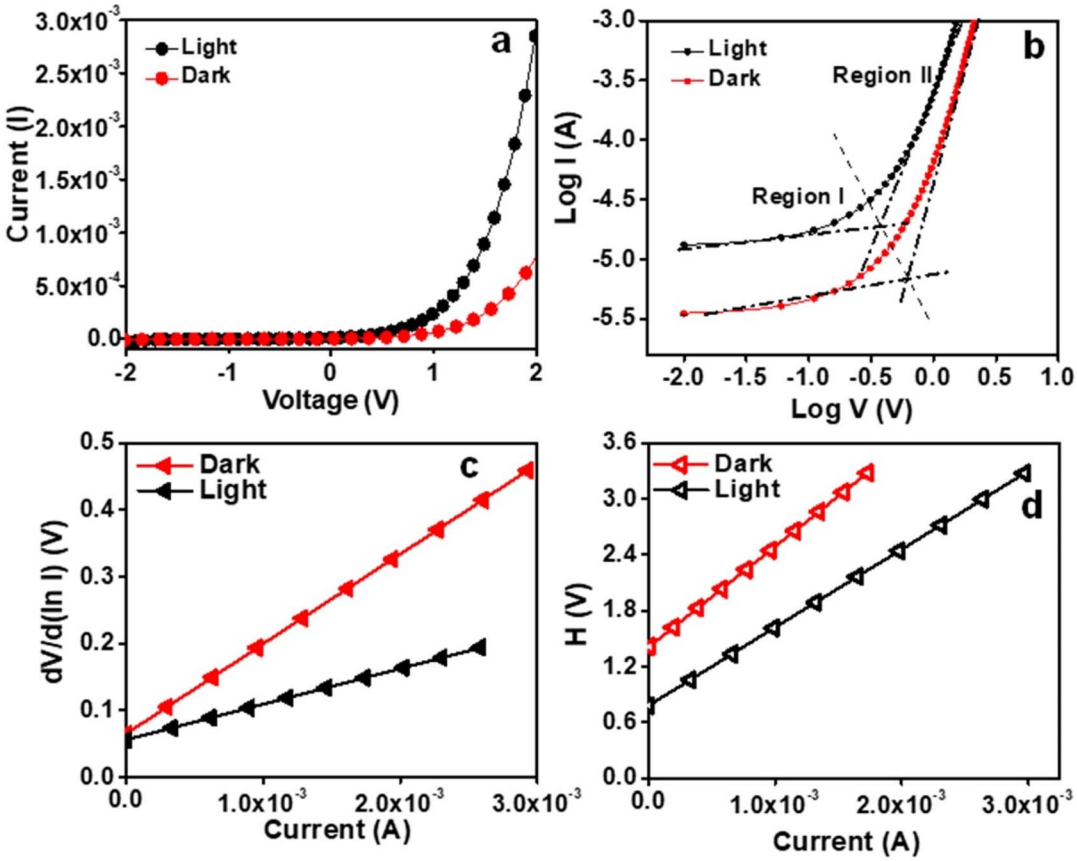

Fig. 7 (a) *I–V* characteristic curves and (b) ln *I vs.* ln *V* curves of the fabricated device under dark and light conditions, (c) d*V*/dln *I vs. I*, and (d) *H vs. I* curves for the device under dark and light conditions.

Table 1 Table indicating the different charge transport parameters of the Zn–inosine thin film device

S. no.	Device name	Conductivity (S m^{-1})	ON/OFF ratio	Series resistance from H (Ω)	Barrier height (eV)	Ideality factor
1	Zn–inosine-dark	2.15×10^{-4}	34.88	1051.29	0.397	2.48
2	Zn–inosine-light	6.15×10^{-4}	49.25	839.11	0.487	2.14

compute the barrier height (ϕ_B). The barrier height was obtained by dividing the intercept of the plot of $H(V)$ *vs.* I with the ideality factor as obtained from the plot of $dV/d\ln I$ *vs.* I. The values of the ideality factor, series resistance, and barrier height (ϕ_B) under both dark and light conditions are summarized in Table 1, which clearly signifies that there is a reduction in the barrier height upon irradiation with UV light, which can be attributed to the formation of photo induced charge carriers and their association close to the conduction band. Thus, it is evident that the Zn–I gel can be utilized for the fabrication of a photosensitive thin film device.

Plotting the I–V curves at the logarithmic scale helps to clearly understand the charge transport events at the MS junction. It was observed that under both dark and photo-illumination conditions, the characteristic $\log(I)$ *vs.* $\log(V)$ curves for the fabricated device exhibited distinct slopes (Fig. 7b). Regions I and II could be used to denote these two areas. In area I, the value of the slope is roughly 1, which denotes the ohmic regime. Here, the generated current follows the relation $I \propto V$. The current produced in region II follows the relation $I \propto V^2$ and has a slope value of approximately 2. This region could be classified as a trap free, space charge limited current (SCLC) regime.[67] The injection of carriers causes a space charge field to spread if the background carriers are smaller than the injected carriers. The current produced in this regime is termed SCLC current, as it is controlled by the space charge field. The performance of the Zn–I gel-based device can be estimated using the SCLC theory.[70] Table 1 contains a list of the various charge transport parameters that control how well a device works while it is turned off and on.

4. Conclusion

In conclusion, the self-assembly of a simple and readily available nucleoside, inosine, triggered by coordination interaction through Zn^{2+} ions leading to the generation of a multifunctional metallo-hydrogel has been demonstrated. The self-assembly of inosine into a stable hydrogel without any external stimuli, such as heating/cooling, indicates the ability of small biological molecules to assemble into ordered superstructures, such as fibers, under the influence of a combination of non-covalent interactions. The coordination interaction between the nucleobase and Zn^{2+} ions, H-bonding interactions, and π–π interactions between the inosine units resulted in the overall self-assembly to form the nanofibers that could trap water molecules to form a gel. The hydrogel showed stimuli responsiveness towards pH and various chemicals. In addition to the thixotropic and injectable behavior, the hydrogel also exhibited self-healing behavior without the aid of any additional healing agent. The transparency of the Zn–I gel could be tuned depending upon the concentration of the NaOH used. The gel demonstrated the unique ability to selectively gel water, which has been harnessed for the separation of water from mixtures containing water and organic solvents or oils. Furthermore, the semiconducting behavior of the gel has been taken advantage of for photosensitive device fabrication based on the Schottky diode interface between a semiconductor and metal. The device exhibited linear rectifying behavior and very good charge transport characteristics. Thus, the Zn–I gel holds potential for applications in wastewater remediation as well as for soft electronic devices.

Data availability

We hereby confirm that we will produce the data reported in the manuscript titled "Multistimuli responsive and self-healing Zn (II)-inosine supramolecular metal–organic gel: phase selective gelation and application as light-responsive Schottky barrier diode" which is submitted to Nanoscale Advances as and when requested.

Conflicts of interest

There are no conflicts of interest to declare.

Acknowledgements

The authors are thankful to MNIT Jaipur for the laboratory and infrastructure. The Materials Research Center (MRC), MNIT Jaipur, is acknowledged for the instrumentation facilities. S. S. and K. R. thank the Ministry of Education (MoE), Government of India (GOI) for a fellowship. B. S. thanks TEQIP-III, MNIT Jaipur for research funding.

References

1 F. Hapiot, S. Menuel and E. Monflier, *ACS Catal.*, 2013, **3**, 1006–1010.
2 X. Sun, S. Agate, K. S. Salem, L. Lucia and L. Pal, *ACS Appl. Bio Mater.*, 2021, **4**, 140–162.
3 Z. Wang, H. Wei, Y. Huang, Y. Wei and J. Chen, *Chem. Soc. Rev.*, 2023, **52**, 2992–3034.
4 A. R. Hirst, B. Escuder, J. F. Miravet and D. K. Smith, *Angew. Chem., Int. Ed.*, 2008, **47**, 8002–8018.
5 S. J. Buwalda, T. Vermonden and W. E. Hennink, *Biomacromolecules*, 2017, **18**, 316–330.
6 J. D. Tang, C. Mura and K. J. Lampe, *J. Am. Chem. Soc.*, 2019, **141**, 4886–4899.

7 F. Zhao, J. Bae, X. Zhou, Y. Guo and G. Yu, *Adv. Mater.*, 2018, **30**, 1801796.
8 B. O. Okesola and D. K. Smith, *Chem. Soc. Rev.*, 2016, **45**, 4226–4251.
9 K. Y. Lee and D. J. Mooney, *Chem. Rev.*, 2001, **101**, 1869–1879.
10 C.-W. Wei, X.-Q. Gong, X.-J. Wang, X.-Z. Yang, S.-Q. Gao and Y.-W. Lin, *New J. Chem.*, 2020, **44**, 7265–7269.
11 C. O. Agubata, C. C. Mbaoji, I. T. Nzekwe, C. Saldías and D. Díaz Díaz, *Appl. Sci.*, 2021, **11**, 6945.
12 O. Ramírez, S. Bonardd, C. Saldías, A. Leiva and D. Díaz Díaz, *Environ. Res.*, 2024, **247**, 118204.
13 S. D. Kurbah and R. A. Lal, *New J. Chem.*, 2020, **44**, 5410–5418.
14 Y. Yang, X. Zhao, J. Yu, X. Chen, X. Chen, C. Cui, J. Zhang, Q. Zhang, Y. Zhang, S. Wang and Y. Cheng, *ACS Appl. Mater. Interfaces*, 2020, **12**, 34161–34169.
15 N. M. Sangeetha and U. Maitra, *Chem. Soc. Rev.*, 2005, **34**, 821–836.
16 X. Du, J. Zhou, J. Shi and B. Xu, *Chem. Rev.*, 2015, **115**, 13165–13307.
17 X. Huang, R. Li, Z. Duan, F. Xu and H. Li, *Soft Matter*, 2022, **18**, 3828–3844.
18 F. Fages, *Angew. Chem., Int. Ed.*, 2006, **45**, 1680–1682.
19 Z. Sun, F. Lv, L. Cao, L. Liu, Y. Zhang and Z. Lu, *Angew. Chem.*, 2015, **127**, 8055–8059.
20 X. Wang, T. He, L. Yang, H. Wu, R. Zhang, Z. Zhang, R. Shen, J. Xiang, Y. Zhang and C. Wei, *Nanoscale*, 2016, **8**, 6479–6483.
21 X. Wang, C. Wei, J. Su, B. He, G. Wen, Y. Lin and Y. Zhang, *Angew. Chem., Int. Ed.*, 2018, **57**, 3504–3508.
22 H. Wu, J. Zheng, A. L. Kjøniksen, W. Wang, Y. Zhang and J. Ma, *Adv. Mater.*, 2019, **31**, 1806204.
23 M. Häring and D. D. Díaz, *Chem. Commun.*, 2016, **52**, 13068–13081.
24 G. Picci, C. Caltagirone, A. Garau, V. Lippolis, J. Milia and J. W. Steed, *Coord. Chem. Rev.*, 2023, **492**, 215225.
25 C. D. Jones and J. W. Steed, *Chem. Soc. Rev.*, 2016, **45**, 6546–6596.
26 Y. Cho, J. H. Lee, J. Jaworski, S. Park, S. S. Lee and J. H. Jung, *New J. Chem.*, 2012, **36**, 32–35.
27 B. Sharma, A. Singh, T. K. Sarma, N. Sardana and A. Pal, *New J. Chem.*, 2018, **42**, 6427–6432.
28 I. Imaz, M. Rubio-Martínez, J. An, I. Solé-Font, N. L. Rosi and D. Maspoch, *Chem. Commun.*, 2011, **47**, 7287–7302.
29 F. Pu, J. Ren and X. Qu, *Chem. Soc. Rev.*, 2018, **47**, 1285–1306.
30 B. Sharma, A. Mahata, S. Mandani, T. K. Sarma and B. Pathak, *RSC Adv.*, 2016, **6**, 62968–62973.
31 B. Sharma, S. Mandani, N. Thakur and T. K. Sarma, *Soft Matter*, 2018, **14**, 5715–5720.
32 B. Sharma, A. Mahata, S. Mandani, N. Thakur, B. Pathak and T. K. Sarma, *New J. Chem.*, 2018, **42**, 17983–17990.
33 I. Imaz, M. Rubio-Martínez, W. J. Saletra, D. B. Amabilino and D. Maspoch, *J. Am. Chem. Soc.*, 2009, **131**, 18222–18223.
34 V. Agarwal, N. Varshney, S. Singh, N. Kumar, A. Chakraborty, B. Sharma, H. C. Jha and T. K. Sarma, *ACS Appl. Bio Mater.*, 2023, **6**, 5018–5029.
35 N. Thakur, B. Sharma, S. Bishnoi, S. Jain, D. Nayak and T. K. Sarma, *ACS Appl. Bio Mater.*, 2019, **2**, 3300–3311.
36 Y. Hu, P. Shen, N. Zeng, L. Wang, D. Yan, L. Cui, K. Yang and C. Zhai, *ACS Appl. Mater. Interfaces*, 2020, **12**, 42285–42293.
37 Y. Ma, B. Li, K. Zhang, Q. Wan, Z. Džolić, Z. Wang and B. Z. Tang, *J. Mater. Chem. C*, 2020, **8**, 13705–13711.
38 M. Cametti, M. Cetina and Z. Džolić, *Dalton Trans.*, 2015, **44**, 7223–7229.
39 S. K. Singh, P. Saha, S. Dey and S. Nandi, *ACS Omega*, 2020, **5**, 8613–8618.
40 A. M. Vibhute, V. Muvvala and K. M. Sureshan, *Angew. Chem.*, 2016, **128**, 7913–7916.
41 A. M. Vibhute and K. M. Sureshan, *ChemSusChem*, 2020, **13**, 5343–5360.
42 N. Thakur, B. Sharma, S. Bishnoi, S. K. Mishra, D. Nayak, A. Kumar and T. K. Sarma, *ACS Sustain. Chem. Eng.*, 2018, **6**, 8659–8671.
43 R. D. Mukhopadhyay and A. Ajayaghosh, *Chem. Soc. Rev.*, 2023, **52**, 8635–8650.
44 S. Majumdar, A. Dey, R. Sahu, G. Lepcha, A. Dey, P. P. Ray and B. Dey, *Mater. Res. Bull.*, 2023, **157**, 112003.
45 K. Karmakar, A. Dey, S. Dhibar, R. Sahu, S. Bhattacharjee, P. Karmakar, P. Chatterjee, A. Mondal and B. Saha, *RSC Adv.*, 2023, **13**, 2561–2569.
46 S. Singh, A. K. Sharma, H. M. Gade, V. Agarwal, R. Nasani, N. Verma and B. Sharma, *Soft Matter*, 2024, **20**, 1025–1035.
47 V. Kumar, R. K. Upadhyay, D. Bano, S. Chandra, P. Kumar Yadav, D. Kumar, S. Jit and S. Hadi Hasan, *Mater. Sci. Eng., B*, 2023, **291**, 116359.
48 B. Pal, S. Dhibar, R. Mukherjee, S. Bhattacharjee, P. P. Ray and B. Saha, *Materials Advances*, 2023, **4**, 3628–3635.
49 M. P. Lepselter and S. M. Sze, *Bell Syst. Tech. J.*, 1968, **47**, 195–208.
50 S. Chand and J. Kumar, *J. Appl. Phys.*, 1997, **82**, 5005–5010.
51 A. Dey, S. Sil, S. Majumdar, R. Sahu, M. Ghosh, G. Lepcha, P. P. Ray and B. Dey, *J. Phys. Chem. Solids*, 2022, **160**, 110300.
52 B. Zhang, X. Dong, Y. Xiong, Q. Zhou, S. Lu, Y. Liao, Y. Yang and H. Wang, *Dalton Trans.*, 2020, **49**, 2827–2832.
53 V. K. Pandey, M. K. Dixit, S. Manneville, C. Bucher and M. Dubey, *J. Mater. Chem. A*, 2017, **5**, 6211–6218.
54 J. Song, E. Khare, L. Rao, M. J. Buehler and N. Holten-Andersen, *Macromol. Rapid Commun.*, 2023, **44**, 2300077.
55 S. Singh, A. Jangir, S. Jain, N. Verma and B. Sharma, *J. Mater. Res.*, 2023, **38**, 3638–3654.
56 H. Sigel, in *Handbook of Metal–Ligand Interactions in Biological Fluids*, ed. G. Berthon, Marcel Dekker, New York, 1995, p. 451.
57 A. Vidyasagar, K. Handore and K. M. Sureshan, *Angew. Chem., Int. Ed.*, 2011, **50**, 8021–8024.
58 C. S. Kesava Raju, B. Pramanik, T. Kar, P. V. C. Rao, N. V. Choudary and R. Ravishankar, *RSC Adv.*, 2016, **6**, 53415–53420.
59 X. Zhang, R. Dai, H. Sun, Y. Zhang, D. Liu, M. Wang, M. Sun and H. Yu, *Mater. Chem. Front.*, 2020, **4**, 222–230.
60 L. Yan, G. Li, Z. Ye, F. Tian and S. Zhang, *Chem. Commun.*, 2014, **50**, 14839–14842.
61 M. Khan, S. Das, A. Roy and S. Roy, *Langmuir*, 2023, **39**, 899–908.

62 R. Tyagi, K. Singh, N. Srivastava and R. Sagar, *Materials Advances*, 2023, **4**, 3929–3950.
63 K. Soundarajan and T. Mohan Das, *Carbohydr. Res.*, 2019, **481**, 60–66.
64 P. I. Scheurle, A. Mähringer, A. C. Jakowetz, P. Hosseini, A. F. Richter, G. Wittstock, D. D. Medina and T. Bein, *Nanoscale*, 2019, **11**, 20949–20955.
65 S. Konar, A. Dey, S. R. Choudhury, K. Das, S. Chatterjee, P. P. Ray, J. Ortega-Castro, A. Frontera and S. Mukhopadhyay, *J. Phys. Chem. C*, 2018, **122**, 8724–8734.
66 S. K. Cheung and N. W. Cheung, *Appl. Phys. Lett.*, 1986, **49**, 85–87.
67 A. Dey, R. Jana, J. Dhar, P. Das and P. P. Ray, *Mater. Today: Proc.*, 2018, **5**, 9958–9964.
68 X. Miao, S. Tongay, M. K. Petterson, K. Berke, A. G. Rinzler, B. R. Appleton and A. F. Hebard, *Nano Lett.*, 2012, **12**, 2745–2750.
69 R. K. Gupta and F. Yakuphanoglu, *Sol. Energy*, 2012, **86**, 1539–1545.
70 A. Dey, S. Middya, R. Jana, M. Das, J. Datta, A. Layek and P. Ray, *J. Mater. Sci.:Mater. Electron.*, 2016, **27**, 6325–6335.